Journal of Zhejiang University SCIENCE A
ISSN 1673-565X (Print); ISSN 1862-1775 (Online)
www.zju.edu.cn/jzus; www.springerlink.com
E-mail: jzus@zju.edu.cn

Adaptive finite element-element-free Galerkin coupling method for bulk metal forming processes*

Lei-chao LIU†, Xiang-huai DONG, Cong-xin LI

(*National Die and Mould CAD Engineering Research Center, Shanghai Jiao Tong University, Shanghai 200030, China*)

†E-mail: liuleichao@yahoo.com.cn

Received Apr. 15, 2008; Revision accepted Sept. 3, 2008; Crosschecked Dec. 29, 2008

Abstract: An adaptive finite element-element-free Galerkin (FE-EFG) coupling method is proposed and developed for the numerical simulation of bulk metal forming processes. This approach is able to adaptively convert distorted FE elements to EFG domain in analysis. A new scheme to implement adaptive conversion and coupling is presented. The coupling method takes both advantages of finite element method (FEM) and meshless methods. It is capable of handling large deformations with no need of remeshing procedures, while it is computationally more efficient than those full meshless methods. The effectiveness of the proposed method is demonstrated with the numerical simulations of the bulk metal forming processes including forging and extrusion.

Key words: Meshless method, Adaptive coupling method, Bulk metal forming, Numerical simulation
doi:10.1631/jzus.A0820286 **Document code:** A **CLC number:** TG3

INTRODUCTION

Meshless methods exhibit their superiority to the finite element method (FEM) in dealing with large deformations, which occur frequently in the bulk metal forming processes. These methods do not need remeshing procedures, and their approximations are constructed entirely in terms of a set of nodes and no explicit mesh is required. It is the reason for these methods that no burdensome remeshing procedures due to mesh distortion are necessary as that in the FEM.

A lot of successful examples of meshless methods applied to the metal forming analysis have been reported. Chen *et al*.(1998a; 1998b) introduced the reproducing kernel particle method (RKPM) to the numerical simulations of ring upsetting and forging-upsetting processes. Several approaches were proposed to facilitate the imposition of essential boundary conditions (Chen and Wang, 2000; Chen *et al*., 2000). Li and Belytschko (2001) presented the total Lagrangian formulation and implementation of the element-free Galerkin method (EFGM) for the analysis of Taylor bar impact, plane-strain upsetting and backward extrusion. The RKPM was implemented in modeling heading and backward extrusion (Xiong *et al*., 2005; Xiong and Martins, 2006).

Despite their superiority, meshless methods are computationally inefficient in comparison to the conventional FEM, which limits their further development and application. Some efforts have been made to couple meshless methods with the FEM. It is intended to implement the meshless methods only in the subdomain where their unique properties are beneficial. The remainder of the domain is modeled by FEM to save unnecessary computational costs. The coupling method may be effective for certain problems such as crack propagation and local metal forming.

Belytschko *et al*.(1995) proposed a coupled finite element-element-free Galerkin (FE-EFG) method with a mixed interpolation in the transition domain.

* Project (No. 50575143) supported by the National Natural Science Foundation of China

Hegen (1996) coupled FEM and EFG with Lagrangian multipliers for elasto-static problems. Xiao and Dhanasekar (2002) developed a collocation approach to couple the FEM and EFGM. Huerta and Fernandez-Mendez (2000) presented a mixed hierarchical approximation based on the FEM and meshless methods. Liu *et al*.(2006) extended the element-free Galerkin-finite element (EFG-FE) coupling method to the analysis of elasto-plastic contact problems. Rabczuk *et al*.(2006) gave an overview of various coupling approaches.

In the coupling methods published, however, the specific domain where each numerical approach is implemented has to be set up manually prior to the analysis. It may be impractical for engineering problems such as metal forming processes, as the domain to be modeled by meshless methods varies dynamically. Therefore, it is significant to develop an adaptive coupling method to avoid this handicap. Karutz *et al*.(2002) presented an adaptive FE/EFG discretization for crack growth. Nevertheless, fragmentary EFG regions are likely to be generated. The method is difficult to be implemented and not suitable for metal forming problems.

In this study, an adaptive FE-EFG coupling method is proposed for bulk metal forming processes. The analysis is started with a full FE model. The severely deformed domain is converted to EFG modeling domain adaptively. A new scheme is presented to implement adaptive coupling procedures, including locating the specific subdomain to be converted and coupling the EFG domain with the retained FE domain. Numerical examples of typical bulk metal forming processes are given.

THEORETICAL BACKGROUND

FE-EFG coupling method

The coupling method proposed in Belytschko *et al*.(1995) is adopted in this research, for its accuracy and applicability. Interface elements Ω_{IE} are introduced to couple the FE domain Ω_{FE} with the EFG domain Ω_{EFG}, as shown in Fig.1.

In the interface element Ω_{IE}, the approximate displacement $\boldsymbol{u}^h(\boldsymbol{x})$ is obtained by interpolating between the FE displacement $\boldsymbol{u}^{\mathrm{FE}}(\boldsymbol{x})$ and the EFG displacement $\boldsymbol{u}^{\mathrm{EFG}}(\boldsymbol{x})$:

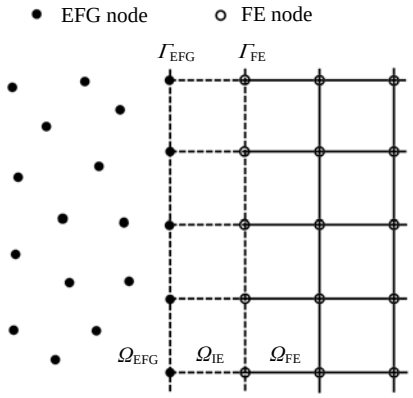

Fig.1 FE-EFG coupling method

$$\boldsymbol{u}^h(\boldsymbol{x}) = [1 - R(\boldsymbol{x})]\boldsymbol{u}^{\mathrm{FE}}(\boldsymbol{x}) + R(\boldsymbol{x})\boldsymbol{u}^{\mathrm{EFG}}(\boldsymbol{x}), \tag{1}$$

where $R(\boldsymbol{x})$, the ramp function, is defined using FE shape functions $N_I(\boldsymbol{x})$:

$$R(\boldsymbol{x}) = \sum_I N_I(\boldsymbol{x}),\ \boldsymbol{x}_I \in \Gamma_{\mathrm{EFG}}. \tag{2}$$

The ramp function is equal to the sum of the FE shape functions associated with the interface element nodes on the EFG boundary Γ_{EFG}.

The interface shape functions can be developed by substituting the FE and EFG displacement approximations into Eq.(1) as follows:

$$\begin{aligned}\boldsymbol{u}^h(\boldsymbol{x}) &= \big[1 - R(\boldsymbol{x})\big]\sum_{I=1}^{4} N_I(\boldsymbol{x})\boldsymbol{u}_I + R(\boldsymbol{x})\sum_{I=1}^{4}\phi_I(\boldsymbol{x})\boldsymbol{u}_I \\ &\equiv \sum_{I=1}^{4}\bar{N}_I(\boldsymbol{x})\boldsymbol{u}_I,\end{aligned} \tag{3}$$

where the interface shape functions $\bar{N}_I(\boldsymbol{x})$ are:

$$\bar{N}_I(\boldsymbol{x}) = \big[1 - R(\boldsymbol{x})\big]N_I(\boldsymbol{x}) + R(\boldsymbol{x})\phi_I(\boldsymbol{x}), \tag{4}$$

where $\phi_I(\boldsymbol{x})$ are EFG shape functions.

Generally, the shape functions of the FE-EFG coupling method $\Psi_I(\boldsymbol{x})$ are summarized as:

$$\Psi_I(\boldsymbol{x}) = \begin{cases} N_I(\boldsymbol{x}), & \boldsymbol{x} \in \Omega_{\mathrm{FE}}; \\ \phi_I(\boldsymbol{x}), & \boldsymbol{x} \in \Omega_{\mathrm{EFG}}; \\ \bar{N}_I(\boldsymbol{x}), & \boldsymbol{x} \in \Omega_{\mathrm{IE}}. \end{cases} \tag{5}$$

Element-free Galerkin method

In the EFGM, the approximant $\boldsymbol{u}^h(\boldsymbol{x})$ for the displacement field $\boldsymbol{u}(\boldsymbol{x})$ is written as:

$$\boldsymbol{u}^h(\boldsymbol{x}) = \boldsymbol{\Phi}(\boldsymbol{x})\boldsymbol{u}, \tag{6}$$

where

$$\boldsymbol{\Phi}(\boldsymbol{x}) = \boldsymbol{p}^{\mathrm{T}}(\boldsymbol{x})\boldsymbol{A}^{-1}(\boldsymbol{x})\boldsymbol{B}(\boldsymbol{x}), \tag{7}$$

$$\boldsymbol{u} = [\boldsymbol{u}_1^{\mathrm{T}},\ \boldsymbol{u}_2^{\mathrm{T}},\ \cdots,\ \boldsymbol{u}_N^{\mathrm{T}}]^{\mathrm{T}}, \tag{8}$$

$$\boldsymbol{A}(\boldsymbol{x}) = \boldsymbol{P}^{\mathrm{T}}\boldsymbol{W}(\boldsymbol{x})\boldsymbol{P}, \tag{9}$$

$$\boldsymbol{B}(\boldsymbol{x}) = \boldsymbol{P}^{\mathrm{T}}\boldsymbol{W}(\boldsymbol{x}), \tag{10}$$

$$\boldsymbol{P} = \left[\boldsymbol{p}(\boldsymbol{x}_1),\ \boldsymbol{p}(\boldsymbol{x}_2),\ ...,\ \boldsymbol{p}(\boldsymbol{x}_N)\right]^{\mathrm{T}}, \tag{11}$$

$$\boldsymbol{W}(\boldsymbol{x}) = \mathrm{diag}\left[w_1(\boldsymbol{x}), w_2(\boldsymbol{x}), ..., w_N(\boldsymbol{x})\right]. \tag{12}$$

In Eq.(11), $\boldsymbol{p}(\boldsymbol{x})$ is the basis vector. Linear basis is used in this study.

$$\boldsymbol{p}(\boldsymbol{x}) = [1, x, y]^{\mathrm{T}}. \tag{13}$$

In Eq.(12), $w_I(\boldsymbol{x})$ is the weight function associated with node I. One of the commonly used weight functions is the cubic spline:

$$w_I(r) = \begin{cases} 2/3 - 4r^2 + 4r^3, & r \le 1/2; \\ 4/3 - 4r + 4r^2 - 4r^3/3, & 1/2 < r \le 1; \\ 0, & r > 1. \end{cases} \tag{14}$$

The normalized distance r is defined as:

$$r = \left|\boldsymbol{x} - \boldsymbol{x}_I\right| / R_I, \tag{15}$$

where R_I is the size of nodal support.

The support associated with a node is determined by the distribution of its neighboring nodes. Sort nodes in order of the increasing distance from node N_I and add the first m nodes to a list $\{N_1, N_2, \cdots, N_m\}$. A vector $\boldsymbol{N}_I\boldsymbol{N}_1$ from N_I to the first node N_1 is drawn. Loop over the other nodes in the list and draw a second vector $\boldsymbol{N}_I\boldsymbol{N}_J$. If the angle between $\boldsymbol{N}_I\boldsymbol{N}_J$ and $\boldsymbol{N}_I\boldsymbol{N}_1$ is within the range from 75° to 105°, stop looping and calculate the distance $R_{IJ} = \sqrt{(x_I - x_J)^2 + (y_I - y_J)^2}$. Thus, the support size R_I is obtained as:

$$R_I = \alpha_{\mathrm{scale}} R_{IJ}, \tag{16}$$

where α_{scale} is a scaling factor provided by users.

Governing equations

Large plastic deformations account for the majority of overall deformations in the bulk metal forming processes. Accordingly, a rigid-plastic material model is adopted. The modified penalty function method is introduced to enforce incompressible constraints and avoid volumetric locking. The energy rate function Π is written as:

$$\Pi = \int_V \bar{\sigma}\,\dot{\bar{\varepsilon}}\,\mathrm{d}V + \frac{\alpha}{2V}\left(\int_V \dot{\varepsilon}_V \mathrm{d}V\right)^2 - \int_{S_{\mathrm{F}}} F_i u_i \mathrm{d}S, \tag{17}$$

where $\bar{\sigma}$ is effective stress, $\dot{\bar{\varepsilon}}$ is effective strain rate, V is volume of integration domain, α is penalty factor, $\dot{\varepsilon}_{\mathrm{V}}$ is volumetric strain rate, F_i is surface traction, u_i is velocity over surface, and S_{F} is frictional boundary.

Based on the variational principle, a set of non-linear equations is obtained. With the Newton-Raphson method, the linear iterative equations are obtained:

$$\begin{aligned}\left[\sum_{\mathrm{c}}\left(\bar{\sigma}\boldsymbol{K}_0 + \frac{\alpha}{V^{\mathrm{c}}}\boldsymbol{Q}\boldsymbol{Q}^{\mathrm{T}}\right)\right]_{n-1} \{\Delta\dot{\boldsymbol{u}}\}_n \\ = \left\{\sum_{\mathrm{c}}\boldsymbol{F}\right\}_{n-1} - \left\{\sum_{\mathrm{c}}\bar{\sigma}\boldsymbol{H}\right\}_{n-1} - \left\{\sum_{\mathrm{c}}\frac{\alpha G}{V^{\mathrm{c}}}\boldsymbol{Q}\right\}_{n-1},\end{aligned} \tag{18}$$

where

$$\boldsymbol{K}_0 = \int_{V^{\mathrm{c}}} \frac{2}{3\dot{\bar{\varepsilon}}}\left(\boldsymbol{B}^{\mathrm{T}}\boldsymbol{B} - \frac{2\boldsymbol{B}^{\mathrm{T}}\boldsymbol{B}\dot{\boldsymbol{u}}^{\mathrm{c}}(\boldsymbol{B}^{\mathrm{T}}\boldsymbol{B}\dot{\boldsymbol{u}}^{\mathrm{c}})^{\mathrm{T}}}{3\dot{\bar{\varepsilon}}^2}\right), \tag{19}$$

$$\boldsymbol{Q} = \int_{V^{\mathrm{c}}} \boldsymbol{B}^{\mathrm{T}}\boldsymbol{C}\mathrm{d}V, \tag{20}$$

$$\boldsymbol{H} = \int_{V^{\mathrm{c}}} \frac{2\boldsymbol{B}^{\mathrm{T}}\boldsymbol{B}\dot{\boldsymbol{u}}^{\mathrm{c}}}{3\dot{\bar{\varepsilon}}}\mathrm{d}V, \tag{21}$$

$$G = \int_{V^{\mathrm{c}}} \boldsymbol{C}^{\mathrm{T}}\boldsymbol{B}\dot{\boldsymbol{u}}^{\mathrm{c}}\mathrm{d}V, \tag{22}$$

$$\dot{\bar{\varepsilon}} = \sqrt{\frac{2}{3}(\boldsymbol{B}\dot{\boldsymbol{u}}^{\mathrm{c}})^{\mathrm{T}}\boldsymbol{B}\dot{\boldsymbol{u}}^{\mathrm{c}}}, \tag{23}$$

$$\boldsymbol{B} = \left[\boldsymbol{B}_1, \boldsymbol{B}_2, ..., \boldsymbol{B}_N\right]. \tag{24}$$

For plane-strain problems,

$$\boldsymbol{B}_I = \begin{bmatrix} \Psi_{I,x} & 0 \\ 0 & \Psi_{I,y} \\ \Psi_{I,y}/\sqrt{2} & \Psi_{I,x}/\sqrt{2} \end{bmatrix}, \tag{25}$$

$$\boldsymbol{C} = [1, 1, 0]^{\mathrm{T}}. \tag{26}$$

For axis-symmetric problems:

$$\boldsymbol{B}_I = \begin{bmatrix} \Psi_{I,r} & 0 \\ 0 & \Psi_{I,z} \\ \Psi_I / r & 0 \\ \Psi_{I,z}/\sqrt{2} & \Psi_{I,r}/\sqrt{2} \end{bmatrix}, \tag{27}$$

$$\boldsymbol{C} = [1, 1, 1, 0]^{\mathrm{T}}. \tag{28}$$

In the above equations, N is the number of nodes whose supports cover the calculating point and V^c denotes the area of a single background cell for 2D problems.

ADAPTIVE FE-EFG COUPLING METHOD

A full FE model is adopted at the beginning of the numerical analysis. The mesh quality is checked constantly. Adaptive conversion and coupling procedures will be implemented if necessary.

Conversion criteria

The conversion criteria are similar to the remeshing criteria in FEM. The conversion is determined by two geometric criteria. One is the level of mesh distortion, and the other is the die interference. Three values are measured for every element. The corresponding limits are predefined according to the characteristics of the given problem. If any of the measured values exceeds the limits, conversion is triggered. Specifically in this study, it is time to carry out conversion if any of the following cases exists: (1) An interior angle is less than 30° or greater than 150°; (2) The ratio aspect is greater than 3.5; (3) The die interference is greater than 5% of the original edge length.

Adaptive coupling procedures

Once the conversion is launched, the converting region is to be determined. For convenience, EFG modeling is implemented in one or two subdomains. It is intended to construct one or two bounding boxes according to the distribution of distorted elements. Any element whose centroid is located inside the box is defined as a converting element, regardless of its distortion level. In this way, no fragmentary EFG regions will be generated and it is applicable for bulk metal forming processes. As shown in Fig.2a, a bounding box is constructed by barely enclosing all nodes of the distorted elements. In some cases, two severely deformed regions may exist and they are separated from each other. A further procedure is carried out to detect this situation. A subsidiary cell with 3 rows and 3 columns is constructed to locate all nodes (Fig.2b). If the middle row or column is not occupied by any node, two separate bounding boxes will be constructed.

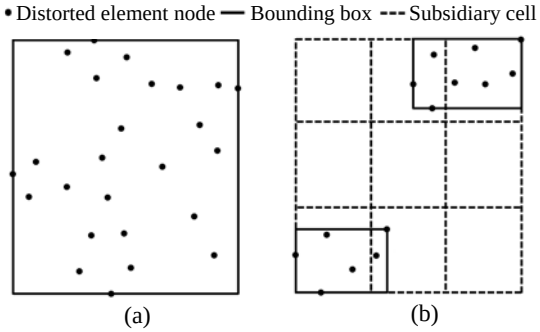

Fig.2 Construction of the bounding boxes. (a) A single box; (b) Two separate boxes

The adaptive coupling procedures are illustrated in Fig.3. Several types of subsidiary elements are defined intermediately to accomplish the adaptive conversion. The two elements with forks are assumed to be the distorted elements (Fig.3a). The bounding box is constructed and the converting elements are defined in the above-mentioned way (Fig.3b). Connective elements and interface elements are defined successively in the outward direction, layer by layer (Fig.3c). Finally, the vertices of the converting elements are converted to EFG nodes. The converting elements and connective elements are removed from the existing mesh (Fig.3d).

Boundary node refinement

The frictional boundary of the workpiece is usually elongated due to the plastic deformation. As a consequence, the node density of deformed boundary

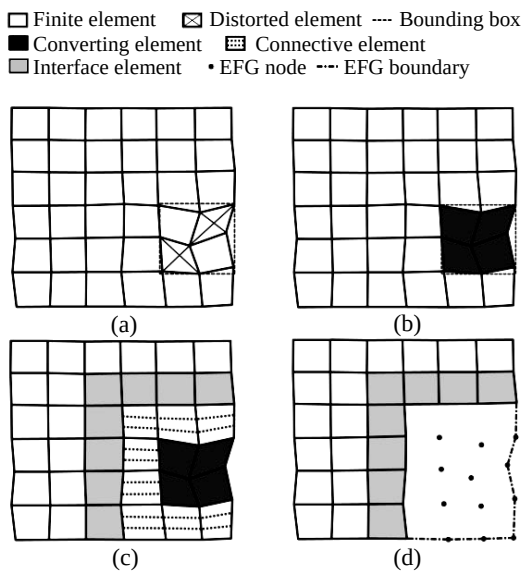

Fig.3 Adaptive coupling procedures. (a) Constructing the bounding box; (b) Defining the converting elements; (c) Identifying different types of elements; (d) Generating EFG regions

decreases and causes intolerable interference with the die. The radius of the die corner is enlarged virtually so that the forming load is underestimated. It is indispensable to refine boundary nodes to capture the metal flow around die corners with desired accuracy.

Since the meshless method do not rely on the explicit meshes, boundary node refinement will be implemented easily by simply inserting new nodes. No topological treatment is required. For any boundary segment, a new node will be generated at the midpoint if any of the following cases exist: (1) The die interference exceeds the predefined value; (2) The segment length exceeds the predefined value.

NUMERICAL EXAMPLES

The adaptive FE-EFG coupling method is validated with numerical examples of bulk metal forming processes including forging and extrusion. Numerical results are compared with FEM solutions obtained by the commercial software DEFORM-2D.

Plane-strain forging

The velocity of the top die is −1.0 mm/s and the bottom die is stationary. The material constitutive model is given by the following expression (unit: MPa):

$$\bar{\sigma} = 68.9\dot{\bar{\varepsilon}}^{0.1}. \tag{29}$$

The billet, with initial dimensions 40 mm×40 mm, is discretized to a full FE model with 441 nodes and 400 elements.

The evolution of metal flow is demonstrated in Fig.4. The elements in contact with the die fillets are converted to EFG regions when the interference exceeds the predefined limit (Fig.4a). Boundary nodes are refined adaptively to match the fillet curvature. The EFG regions expand with further deformation (Figs.4b, 4c, and 4d).

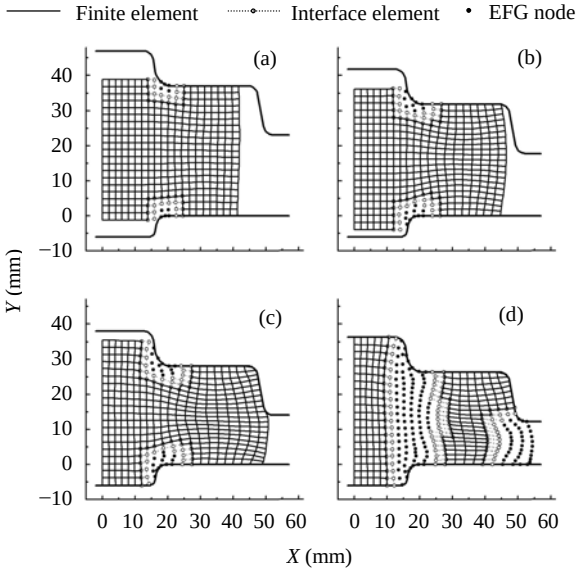

Fig.4 Evolution of metal flow at different strokes. (a) 2.96 mm; (b) 8.21 mm; (c) 11.97 mm; (d) 13.72 mm

Comparisons of effective strain contours, effective stress contours and load-stroke curves are plotted in Figs.5~7, respectively. The results obtained by the coupling method are close to FEM ones.

The computational efficiency of the adaptive coupling method was investigated in comparison with the EFGM, a representative of meshless methods. With the same number of discretized nodes, two numerical programs using each method were executed on a personal computer with a Pentium D 2.8 GHz processor. The computer time recorded is 1246.6 s and 400.8 s for EFGM and the coupling method, respectively. The adaptive coupling method costs much less time than the full meshless method.

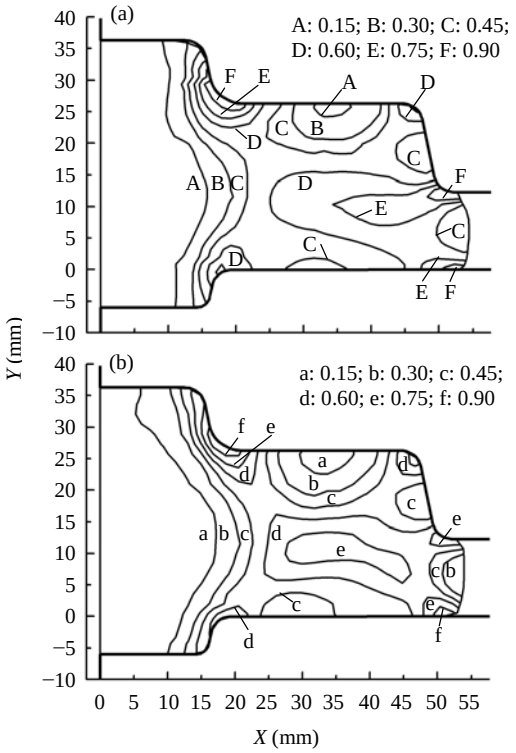

Fig.5 Comparison of effective strain contours. (a) Coupling method; (b) FEM

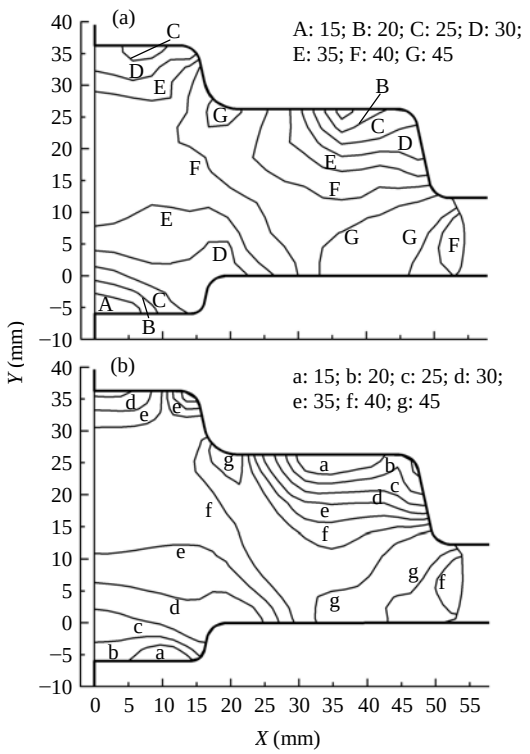

Fig.6 Comparison of effective stress contours (unit: MPa). (a) Coupling method; (b) FEM

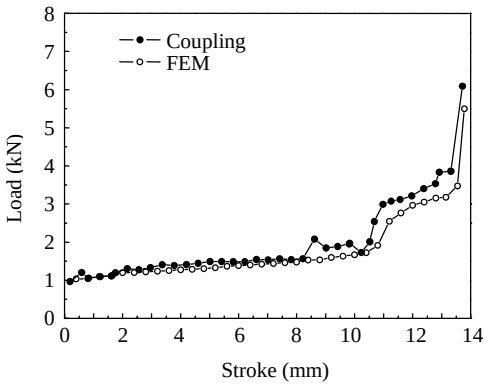

Fig.7 Comparison of load-stroke curves

Axis-symmetric forward-backward extrusion

The cylindrical billet is 20 mm in radius and 18 mm in height. It is discretized to an FE model with 399 nodes and 360 elements. The stress-strain curve of the material is:

$$\bar{\sigma} = 209.0\bar{\varepsilon}^{0.122}. \quad (30)$$

The deformed numerical model at different stages in the simulation is shown in Fig.8. As shown in Fig.8a, the main deformations concentrate on the regions in contact with the tool fillets at the early stage. Once the distortion of the contacting elements exceeds the conversion criteria, two EFG modeling regions are generated successively (Fig.8b and 8c). The EFG area accounts for only a portion of the whole area at the later stage (Fig.8d). Considerable computation time is expected to be saved by implementing the adaptive coupling method.

Strain contours and stress contours at the ram displacement of 2.84 mm are shown in Fig.9 and Fig.10, respectively. The two figures are quite identical. To analyze the flow pattern of the extruded metal, a number of points are sampled near the two die exits. Fig.11 plots the distribution of axial velocity V_z at the height of Z=2.0 mm and Z=13.0 mm. The curves are in good agreement with FEM ones.

The CPU time used by the coupling method is 163.6 s, only 15.4% of that by EFGM (1059.8 s). The time saving is considerable.

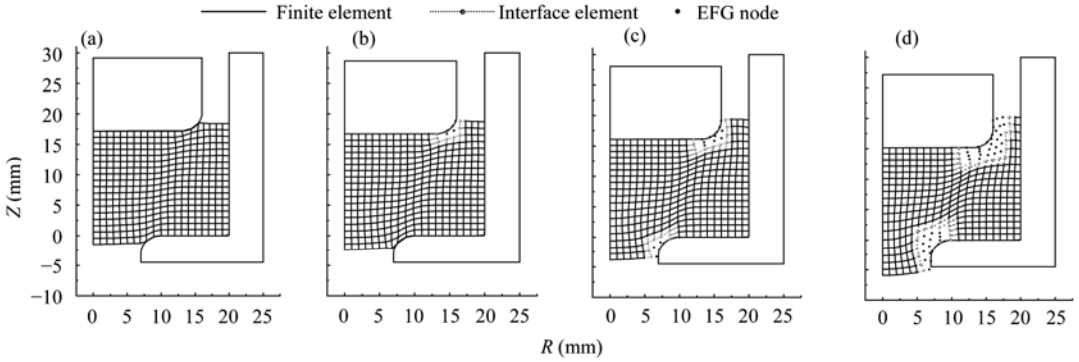

Fig.8 Evolution of metal flow at different ram displacements. (a) 0.84 mm; (b) 1.30 mm; (c) 1.93 mm; (d) 2.84 mm

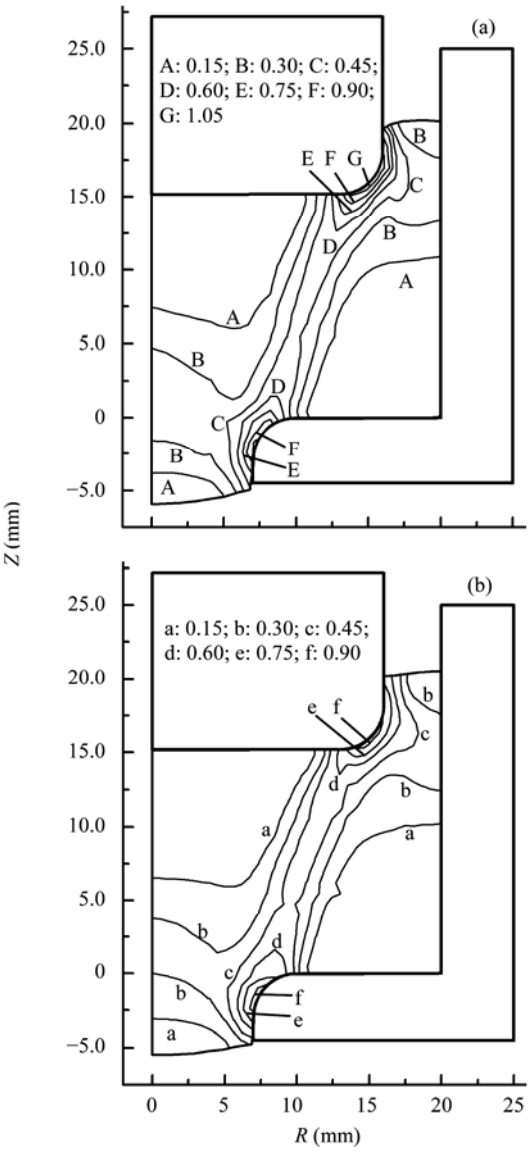

Fig.9 Comparison of effective strain contours. (a) Coupling method; (b) FEM

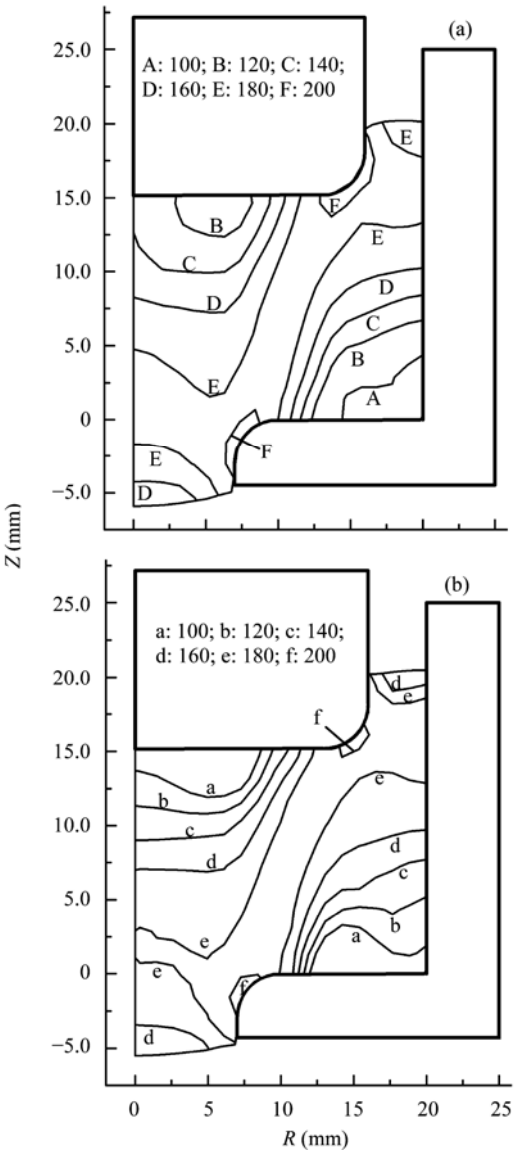

Fig.10 Comparison of effective stress contours (unit: MPa). (a) Coupling method; (b) FEM

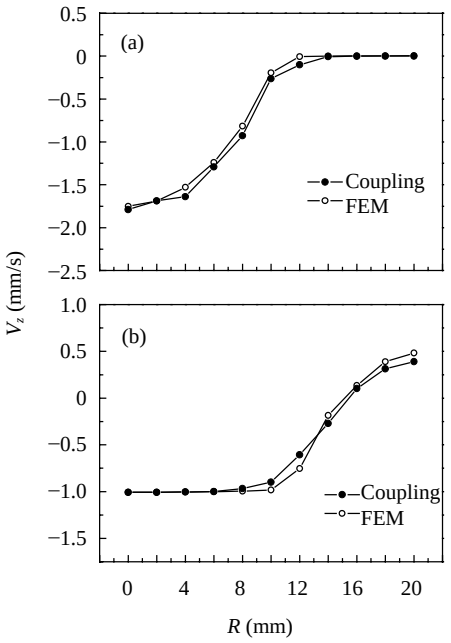

Fig.11 Comparison of axial velocity distribution at ram displacement of 2.84 mm. (a) Z=2.0 mm; (b) Z=13.0 mm

CONCLUSION

An adaptive FE-EFG coupling method is proposed and applied to the numerical simulation of bulk metal forming processes. The adaptive conversion and coupling procedures are presented in detail. This method is able to convert the distorted FE domain to the EFG domain adaptively in the analysis.

The proposed method is validated with the simulations of plane-strain forging and axis-symmetric forward-backward extrusion. The simulation succeeded in running continuously without the need of remeshing procedures as that in the conventional FEM. The numerical results are in good agreement with FEM solutions, while the computation time is reduced considerably compared to the full meshless methods.

References

Belytschko, T., Organ, D., Krongauz, Y., 1995. A coupled finite element-element-free Galerkin method. *Computational Mechanics*, **17**(3):186-195. [doi:10.1007/S004660050102]

Chen, J.S., Wang, H.P., 2000. New boundary condition treatments in meshfree computation of contact problems. *Computer Methods in Applied Mechanics and Engineering*, **187**(3-4):441-468. [doi:10.1016/S0045-7825(00)80004-3]

Chen, J.S., Pan, C., Roque, C.O.M.L., Wang, H.P., 1998a. A Lagrangian reproducing kernel particle method for metal forming analysis. *Computational Mechanics*, **22**(3): 289-307. [doi:10.1007/S004660050361]

Chen, J.S., Roque, C.M.O.L., Pan, C., Button, S.T., 1998b. Analysis of metal forming process based on meshless method. *Journal of Materials Processing Technology*, **80-81**:642-646. [doi:10.1016/S0924-0136(98)00171-X]

Chen, J.S., Wang, H.P., Yoon, S., You, Y., 2000. Some recent improvements in meshfree methods for incompressible finite elasticity boundary value problems. *Computational Mechanics*, **25**(2-3):137-156. [doi:10.1007/S004660050465]

Hegen, D., 1996. Element-free Galerkin methods in combination with finite element approaches. *Computer Methods in Applied Mechanics and Engineering*, **135**(1-2):143-166. [doi:10.1016/0045-7825(96)00994-2]

Huerta, A., Fernandez-Mendez, S., 2000. Enrichment and coupling of the finite element and meshless methods. *International Journal for Numerical Methods in Engineering*, **48**(11):1615-1636. [doi:10.1002/1097-0207(20000820)48:11<1615::AID-NME883>3.0.CO;2-S]

Karutz, H., Chudoba, R., Kratiz, W.B., 2002. Automatic adaptive generation of a coupled finite element/ element-free Galerkin discretization. *Finite Elements in Analysis and Design*, **38**(11):1075-1091. [doi:10.1016/S0168-874X(02)00052-5]

Li, G.Y., Belytschko, T., 2001. Element-free Galerkin method for contact problems in metal forming analysis. *Engineering Computations*, **18**(1-2):62-78. [doi:10.1108/02644400110365806]

Liu, T.X., Liu, G., Wang, Q.J., 2006. An element-free Galerkin-finite element coupling method for elasto-plastic contact problems. *Journal of Tribology*, **128**(1):1-9. [doi:10.1115/1.1843134]

Rabczuk, T., Xiao, S.P., Sauer, M., 2006. Coupling of mesh-free methods with finite elements: basic concepts and test results. *Communications in Numerical Methods in Engineering*, **22**(10):1031-1065. [doi:10.1002/cnm.871]

Xiao, Q.Z., Dhanasekar, M., 2002. Coupling of FE and EFG using collocation approach. *Advances in Engineering Software*, **33**(7-10):507-515. [doi:10.1016/S0965-9978(02)00069-8]

Xiong, S.W., Martins, P.A.F., 2006. Numerical solution of bulk metal forming processes by the reproducing kernel particle method. *Journal of Materials Processing Technology*, **177**(1-3):49-52. [doi:10.1016/j.jmatprotec.2006.03.204]

Xiong, S.W., Liu, W.K., Cao, J., Li, C.S., 2005. Simulation of bulk metal forming processes using the reproducing kernel particle method. *Computers & Structures*, **83**(8-9):574-587. [doi:10.1016/j.compstruc.2004.11.008]